Soft Matter

RSC Publishing

PAPER

View Article Online
View Journal | View Issue

Cite this: *Soft Matter*, 2013, **9**, 4015

Self-consistent field theory study of the solvation effect in polyelectrolyte solutions: beyond the Poisson–Boltzmann model†

Liquan Wang, Jiaping Lin* and Qian Zhang

We developed a self-consistent field theory to study the solvation effect in polyelectrolyte solutions by taking into account the dipolar feature of polar solvents. A Langevin Poisson–Boltzmann equation describing the electrostatic interactions was derived at the mean-field level and numerically solved by an *ad-hoc* direct spectral algorithm. This method enables the SCFT to be implemented in real space. The developed self-consistent field model was applied to salt-free concentrated solutions of diblock polyampholytes and charged–neutral diblock copolymers. It was found that an increase in the magnitude of dipole moments can lead to an increase in the effective dielectric constant and thereby the change of the phase behaviors. As the magnitude of the dipole moment increases, the segregation between dissimilar blocks becomes strong, and the lamellar spacing undergoes a non-monotonic variation where the spacing first decreases and then increases to reach a plateau. The proposed calculation method can be extended to the solutions of polyelectrolytes with different architectures and polar solutions containing added salts.

Received 15th August 2012
Accepted 4th February 2013

DOI: 10.1039/c3sm27891c

www.rsc.org/softmatter

Introduction

Polyelectrolytes, bearing a number of dissociated ionic groups, are one of the most important classes of polymers due to their wide industrial applications and bio-related characteristics.[1–3] Notable examples of such systems include proteins, nucleic acids, and synthetic polymers like polyacrylic acid.[4] Until now, polyelectrolytes have been the least understood polymeric systems, since the polymeric systems involve a complex interplay between short-range excluded volume interactions and long-range Coulomb interactions. Meanwhile, the polyelectrolyte solution is electrically neutral, where the polyelectrolytes are embedded in an environment comprising the counterions, polar solvents, and other dissociated salt ions. Therefore, there exists an additional interplay among the large polyelectrolyte molecules, solvent molecules, and small ions that are coupled electrostatically. In view of this complex interplay, it is a challenge to develop theoretical descriptions of the thermodynamic properties of the polyelectrolyte solutions, in an effort to explain some trends observed in experiments and make predictions.

A self-consistent field theory (SCFT), coupled with the Poisson–Boltzmann (PB) theory, has been developed to describe the polyelectrolyte systems in the absence/presence of added salt ions. The SCFT, based on the field theory first proposed by Edwards,[5,6] has been a standard technique for investigating the phase behaviors of neutral polymeric systems.[7–15] In the framework of SCFT, the long-range Coulomb interactions are converted to the short-range interactions through a Hubbard–Stratonovich transformation.[16] It therefore exhibits advantages over particle-based simulations in some aspects like computational expense. The SCFT approach for polyelectrolyte systems was first proposed by Borukhov *et al.* for semidilute solutions of polyelectrolytes and polyampholytes possessing various charge distributions,[17,18] and further generalized by Shi and Noolandi to multicomponent polyelectrolyte systems.[19] This approach was also applied to study the phase separation of block polyelectrolytes,[20–23] adsorption of polyelectrolytes on a charged surface,[24–26] polymer brushes,[27,28] confinement effects,[29] counterion adsorption,[30] and so on.

In most of the previous studies, the polyelectrolyte systems were modeled with a homogeneous and isotropic dielectric constant, and the strong dielectric response of polar solvents (*e.g.*, water) around charges was not taken into consideration. As a matter of fact, the polar molecules like water could orient themselves close to charged objects, giving rise to hydration shells and inhomogeneous dielectric response. It also means that the long-range Coulomb forces can be partly screened by

Shanghai Key Laboratory of Advanced Polymeric Materials, Key Laboratory for Ultrafine Materials of Ministry of Education, State Key Laboratory of Bioreactor Engineering, School of Materials Science and Engineering, East China University of Science and Technology, Shanghai 200237, China. E-mail: jlin@ecust.edu.cn; Tel: +86-21-64253370

† Electronic supplementary information (ESI) available: Effect of ion volume on phase behaviors, effect of the magnitude of the dipole moment on ODT, and connection between our method and the SCFT involving only a volume fraction weighted dielectric constant and no explicit ion–dipole interaction. See DOI: 10.1039/c3sm27891c

polar solvents. This screening effect is essential to gain insight into the behavior of the polyelectrolytes in solutions, and therefore cannot be ignored.[1,2] Wang *et al.* have considered the influence of the inhomogeneous dielectric constant on the phase behavior of polyelectrolyte solutions.[20] In their assumption, the dielectric constant was treated as a position-dependent parameter by incorporating it with the local densities of the polyelectrolytes and solvents. This assumption, however, still does not explicitly take into account the screening effect resulting from the orientational ordering of polar solvents. Although the spatially varying dielectric constant may involve the ion–solvent interactions implicitly, its validity should be tested and how to associate the implicit dielectric constant with the ion–solvent interactions is unclear. Therefore, the question still remains as to how the presence of polar solvents such as water influences the phase behavior of the polyelectrolytes in detail.

To address this problem, we assumed the polar solvents explicitly as freely orienting Langevin dipoles, as proposed by Orland and Iglič *et al.*[31–36] Based on this assumption, a SCFT coupled with the Langevin Poisson–Boltzmann (LPB) equation was developed rigorously. The LPB equation, which can describe the electrostatic interactions between the charged objects and polar solvents, was solved using an *ad-hoc* direct spectral method,[37] and the SCFT equations were solved by employing a real-space numerical scheme.[38,39] The numerical method for studying the polyelectrolytes in polar solvents was found to be as efficient as that for neutral polymeric systems. In the present work, we took two polyelectrolyte systems as examples, namely, diblock polyampholyte solutions and charged–neutral diblock polyelectrolyte solutions, and investigated the effect of the magnitude of the dipole moment on their phase behaviors including density distribution and lamellar spacing. It was found that the increase of the magnitude of the dipole moment can lead to a screening of charges, and thereby influences the phase behaviors of polyelectrolytes. The results indicate that our method might be a feasible tool for studying the solvation effect in polyelectrolyte solutions.

Theoretical method

SCFT formalism

In this work, we considered a system of volume V consisting of n_P diblock polyelectrolytes and n_S polar solvents, as shown in Fig. 1. Each copolymer processes N total statistical segments with N_A segments A and N_B segments B. The volume fractions of A and B blocks in the diblock polyelectrolytes are represented as f and $1-f$, respectively. The bulk densities, *i.e.*, number per unit volume, of polymer segments, solvents, and ions are denoted as ρ_P^0, ρ_S^0, and $\rho_\pm^0$, respectively. We assumed that all the polymer segments have the same bulk density as the solvents, *i.e.*, $\rho_P^0 = \rho_S^0 = \rho_0$ (ρ_0 is defined as a reference density). In addition, $\nu_\pm = \rho_0/\rho_\pm^0$ is introduced to represent the ratio of the polymer segment density to ion density. Since the ions are much smaller than the polymer segments (or solvents), the value of $\nu_\pm$ should be much smaller than 1. The subscripts A, B, S, +, and – in the variables are used to represent the A blocks, B blocks, polar solvents, cations, and anions, respectively. The valence number of charged species is denoted as $z_k (k = \mathrm{A}, \mathrm{B}, +, -)$, and the corresponding charge is $z_k e$ (e is elementary charge). The polar solvent molecule is described as the Langevin dipoles with a non-zero dipole moment $\boldsymbol{p}$ (see Fig. 1). The procedure of deriving SCFT equations is similar to that in the work of Shi and Noolandi.[19] In the following, we aim to show how the Langevin Poisson–Boltzmann equation including the ion–solvent interactions is derived and coupled with the SCFT equations.

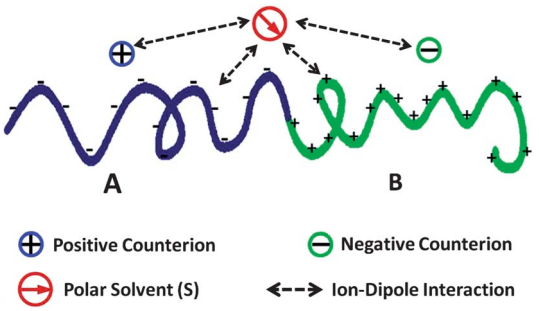

Fig. 1 Sketch of the diblock polyelectrolytes in polar solvents. The system contains the polyelectrolytes, positive counterions released from A blocks, negative counterions released from B blocks, and polar solvents modeled as permanent Langevin dipoles.

The partition function of the diblock polyelectrolytes with annealed charge distributions in polar solvents can be written in terms of a functional integral over all the chain conformation, the positions and orientations of polar solvents, and the ion positions

$$\begin{aligned} Z = & \prod_j \left(\frac{\zeta_j^{n_j}}{n_j!} \right) \left[\prod_{k=1}^{n_P} \sum_{\{\theta_k(s)\}} P(\{\theta_k(s)\}) \right] \left(\prod_{k=1}^{n_P} \int D\boldsymbol{R}_k \right) \\ & \times \prod_I \left(\prod_{k=1}^{n_I} \int \mathrm{d}\boldsymbol{r}_k^I \right) \left(\prod_{k=1}^{n_S} \int \mathrm{d}\boldsymbol{r}_k^S \int \mathrm{d}\boldsymbol{p}_k \right) \\ & \times \int D\psi \exp(-\beta H) \delta \left(\int \mathrm{d}\boldsymbol{r} \hat{\phi}_e(\boldsymbol{r}) \right) \prod_{\boldsymbol{r}} \delta \left[\sum_j \hat{\phi}_j(\boldsymbol{r}) - 1 \right] \end{aligned} \quad (1)$$

where ζ_j is the partition function of a single molecule due to the kinetic energy. $\theta_k(s)$ denotes the dissociation of the s^{th} segment, k^{th} polymer chain. $P(\{\theta_k(s)\})$ is the probability of a particular charge distribution, and $\sum_{\{\theta_k(s)\}}$ is a summation over the charge distributions for the k^{th} chain. The subscripts j and I denote all the species in the system and small ions (+ and −), respectively. $\boldsymbol{R}_k$ represents the space curve of the k^{th} polymer chain, $\boldsymbol{r}_k^{\mathrm{I}}$ represents the position of the k^{th} ion of type I, and $\boldsymbol{r}_k^{\mathrm{S}}$ represents the position of the k^{th} solvent molecule. $\beta = \frac{1}{k_B T}$ is the inverse of the thermal energy, where k_B and T are the Boltzmann constant and temperature, respectively. In eqn (1), the Hamiltonian H of the system consists of three parts

$$H = H_0 + H_1 + H_2 \quad (2)$$

Here, H_0 describes the elastic energy of Gaussian chains (b is the statistical segment length)

$$H_0 = \sum_{k=1}^{n_P} \frac{3}{2\beta b^2} \int_0^N \mathrm{d}s \left| \frac{\mathrm{d}\boldsymbol{R}_k(s)}{\mathrm{d}s} \right|^2 \tag{3}$$

H_1 is the short-range interaction energy of the system

$$H_1 = \frac{\rho_0}{2\beta} \sum_{\substack{j,j' \\ j \neq j'}} \int \mathrm{d}\boldsymbol{r} \chi_{jj'} \hat{\phi}_j(\boldsymbol{r}) \hat{\phi}_{j'}(\boldsymbol{r}) \tag{4}$$

where the Flory–Huggins parameter $\chi_{jj'}(j,j' = \mathrm{A}, \mathrm{B}, \mathrm{C}, +, -)$ is a dimensionless phenomenological parameter describing the interaction strength between j and j' species (in unit of $k_\mathrm{B}T$). Thus, the interaction energy H_1 is independent of the temperature T. H_2 is the electrostatic energy of the system

$$H_2 = \int \mathrm{d}\boldsymbol{r} \hat{\phi}_\mathrm{e}(\boldsymbol{r}) \psi(\boldsymbol{r}) - \int \mathrm{d}\boldsymbol{r} \frac{\varepsilon(\boldsymbol{r})}{8\pi} |\nabla \psi(\boldsymbol{r})|^2 \tag{5}$$

where $\hat{\phi}_\mathrm{e}(\boldsymbol{r})$, $\psi(\boldsymbol{r})$, and $\varepsilon(\boldsymbol{r})$ are the total charge density, electrostatic potential, and dielectric constant at position $\boldsymbol{r}$, respectively. Here, the solvents are considered as explicit permanent dipoles in a background medium formed by the polymers and solvents. The relevant density operators are defined as

$$\begin{aligned}
\hat{\phi}_\mathrm{A}(\boldsymbol{r}) &= \frac{1}{\rho_0} \sum_{k=1}^{n_P} \int_0^{N_\mathrm{A}} \mathrm{d}s \delta\big(\boldsymbol{r} - \boldsymbol{R}_k(s)\big) \\
\hat{\phi}_\mathrm{B}(\boldsymbol{r}) &= \frac{1}{\rho_0} \sum_{k=1}^{n_P} \int_{N_\mathrm{A}}^{N} \mathrm{d}s \delta\big(\boldsymbol{r} - \boldsymbol{R}_k(s)\big) \\
\hat{\phi}_\mathrm{S}(\boldsymbol{r}) &= \frac{1}{\rho_0} \sum_{k=1}^{n_S} \delta\big(\boldsymbol{r} - \boldsymbol{r}_k^\mathrm{S}\big) \\
\hat{\phi}_\pm(\boldsymbol{r}) &= \frac{\nu_\pm}{\rho_0} \sum_{k=1}^{n_\pm} \delta\big(\boldsymbol{r} - \boldsymbol{r}_k^\pm\big)
\end{aligned} \tag{6}$$

The total charge is a sum over the contributions from the polyions, ions, and solvents

$$\begin{aligned}
\hat{\phi}_\mathrm{e}(\boldsymbol{r}) = e \sum_{k=1}^{n_P} \int_0^N \mathrm{d}s z_P \theta_k(s) \delta(\boldsymbol{r} - \boldsymbol{R}_k(s)) + \sum_{I=+,-} \sum_k^{n_I} z_I e \delta(\boldsymbol{r} - \boldsymbol{r}_k^I) \\
- \sum_k^{n_S} \boldsymbol{p}_k \cdot \nabla \delta(\boldsymbol{r} - \boldsymbol{r}_k^S)
\end{aligned} \tag{7}$$

$$1 = \prod_j \int D\phi_j D(\rho_0 \omega_j) \exp\left\{ \int \mathrm{d}\boldsymbol{r} \rho_0 \omega_j(\boldsymbol{r}) \left[\phi_j(\boldsymbol{r}) - \hat{\phi}_j(\boldsymbol{r}) \right] \right\} \tag{8}$$

it introduces a density field $\phi_j(\boldsymbol{r})$ constrained to $\hat{\phi}_j(\boldsymbol{r})$ and an effective chemical potential field $\omega_j(\boldsymbol{r})$ conjugated to the density fields. Next, we inserted eqn (6) and the following two δ functions into eqn (1)

$$\delta\left(\int \mathrm{d}\boldsymbol{r} \hat{\phi}_\mathrm{e}(\boldsymbol{r})\right) = \int \mathrm{d}\eta \exp\left\{ -\eta \int \mathrm{d}\boldsymbol{r} \hat{\phi}_\mathrm{e}(\boldsymbol{r}) \right\} \tag{9}$$

$$\prod_{\boldsymbol{r}} \delta\left(\rho_0 \left[\sum_j \phi_j(\boldsymbol{r}) - 1 \right] \right) = \int D\xi \exp\left\{ -\int \mathrm{d}\boldsymbol{r} \xi(\boldsymbol{r}) \rho_0 \left[\sum_j \phi_j(\boldsymbol{r}) - 1 \right] \right\} \tag{10}$$

where the Lagrange multipliers η and $\xi(\boldsymbol{r})$ are introduced to ensure the charge neutrality and incompressibility of the systems, respectively. The η can be absorbed into $\psi(\boldsymbol{r})$, *i.e.*, $\int D\psi \int \mathrm{d}\eta f(\psi(\boldsymbol{r}) + \eta) \propto \int D\psi f(\psi(\boldsymbol{r}))$. The partition function of the system can then be written as

$$Z \propto \int \prod_j \left(D\phi_j D\omega_j \right) D\psi D\xi \exp(-\beta F) \tag{11}$$

where

$$\begin{aligned}
\frac{\beta N F}{\rho_0 V} = \frac{1}{V} \int \mathrm{d}\boldsymbol{r} \Bigg\{ \frac{1}{2} \sum_{\substack{j,j' \\ j \neq j'}} \chi_{jj'} N \phi_j(\boldsymbol{r}) \phi_{j'}(\boldsymbol{r}) - N \sum_j \omega_j(\boldsymbol{r}) \phi_j(\boldsymbol{r}) \\
- \frac{N\varepsilon(\boldsymbol{r})}{8\pi\rho_0\beta} |\nabla \varphi(\boldsymbol{r})|^2 + N\xi(\boldsymbol{r}) \left[\sum_j \phi_j(\boldsymbol{r}) - 1 \right] \Bigg\} - c_\mathrm{p} \ln\left(\frac{Q_\mathrm{P}}{V} \right) \\
- \sum_{I=+,-} N c_I \ln\left(\frac{Q_I}{V} \right) - N c_\mathrm{S} \ln\left(\frac{Q_\mathrm{S}}{V} \right)
\end{aligned} \tag{12}$$

Here, $c_\mathrm{p} = n_\mathrm{P}N/\rho_0 V$, $c_\pm = n_\pm/\rho_0 V$, and $c_\mathrm{S} = n_\mathrm{S}/\rho_0 V$ are the volume-averaged densities for the polyelectrolytes, small ions, and solvents, respectively. They represent the number of molecules in volume V. $\varphi(\boldsymbol{r})$ is defined as $\varphi(\boldsymbol{r}) = \beta\psi(\boldsymbol{r})$. The dielectric constant $\varepsilon(\boldsymbol{r})$ is assumed as a volume fraction weighted average, *i.e.*, $\varepsilon(\boldsymbol{r}) = \sum_j \phi_j(\boldsymbol{r}) \varepsilon_j$ (ε_j is the dielectric constant of the species j).[20] Q_P is the partition function of a single polyelectrolyte chain

$$Q_\mathrm{P} = \frac{\displaystyle \int D\boldsymbol{R} \sum_{\{\theta(s)\}} P(\{\theta(s)\}) \exp\left\{ -\int_0^N \mathrm{d}s \left[\frac{3}{2b^2} \left| \frac{\mathrm{d}\boldsymbol{R}(s)}{\mathrm{d}s} \right|^2 + \omega_k(\boldsymbol{R}(s)) + \theta(s) z_k e \varphi(\boldsymbol{R}(s)) \right] \right\}}{\displaystyle \int D\boldsymbol{R} \exp\left\{ -\int_0^N \mathrm{d}s \frac{3}{2b^2} \left| \frac{\mathrm{d}\boldsymbol{R}(s)}{\mathrm{d}s} \right|^2 \right\}} \tag{13}$$

where $z_\mathrm{P} = z_\mathrm{A}$ if $s \leq N_\mathrm{A}$ and $z_\mathrm{P} = z_\mathrm{B}$ if $s \geq N_\mathrm{A}$.

In eqn (1), the first δ function represents the charge neutrality of the whole system, and the second δ function imposes the incompressibility at all positions $\boldsymbol{r}$. Through inserting the following identity into eqn (1),

where k is A if $s \leq N_\mathrm{A}$ and B if $s \geq N_\mathrm{A}$. The annealed charge distribution can be written in the form $P(\{\theta(s)\}) = \Pi_s p(\theta(s),s)$. For the smeared charge distributions, the charges are fixed and smeared along the chain so that $p(\theta(s),s) = \delta(\theta(s) - \alpha_k)$, where α_k is the charge fraction of the polymer segment of

type k. By inserting the above relations into eqn (13), the Q_P for the smeared charge distributions can be written as

$$Q_P = \frac{\int D\boldsymbol{R} \exp\left\{-\int_0^N \mathrm{d}s\left[\frac{3}{2b^2}\left|\frac{\mathrm{d}\boldsymbol{R}(s)}{\mathrm{d}s}\right|^2 + \omega_k(\boldsymbol{R}(s)) + \alpha_k z_k e\varphi(\boldsymbol{R}(s))\right]\right\}}{\int D\boldsymbol{R} \exp\left\{-\int_0^N \mathrm{d}s \frac{3}{2b^2}\left|\frac{\mathrm{d}\boldsymbol{R}(s)}{\mathrm{d}s}\right|^2\right\}} \tag{14}$$

$Q_\pm$ is the partition function of a single ion

$$Q_\pm = \int \mathrm{d}\boldsymbol{r} \exp[-\nu_\pm\omega_\pm(\boldsymbol{r}) - z_\pm e\varphi(\boldsymbol{r})] \tag{15}$$

Q_S is the partition function of a single solvent

$$\begin{aligned} Q_S &= \frac{1}{4\pi}\int \mathrm{d}\boldsymbol{r}\int \mathrm{d}\boldsymbol{p} \exp[-\omega_S(\boldsymbol{r}) - \boldsymbol{p}\cdot\nabla\varphi(\boldsymbol{r})] \\ &= \int \mathrm{d}\boldsymbol{r} \exp[-\omega_S(\boldsymbol{r})]\ \frac{\sinh(p|\nabla\varphi(\boldsymbol{r})|)}{p|\nabla\varphi(\boldsymbol{r})|} \end{aligned} \tag{16}$$

The mean-field equations are obtained by the saddle-point approximation, where one sets $\delta F/\delta\phi_j = 0$, $\delta F/\delta\omega_j = 0$, and $\delta F/\delta\xi_j = 0$. The SCFT equations can be written as

$$\omega_j(\boldsymbol{r}) = \sum_{\substack{j,j' \\ j\neq j'}} \chi_{jj'}\phi_{j'}(\boldsymbol{r}) + \xi(\boldsymbol{r}) - \frac{\varepsilon_j}{8\pi\rho_0\beta}|\nabla\varphi(\boldsymbol{r})|^2 \tag{17}$$

$$\phi_\pm(\boldsymbol{r}) = \frac{Vc_\pm\nu_\pm}{Q_\pm}\exp[-\nu_\pm\omega_\pm(\boldsymbol{r}) - z_\pm e\varphi(\boldsymbol{r})] \tag{18}$$

$$\phi_A(\boldsymbol{r}) = \frac{Vc_P}{Q_P}\int_0^f \mathrm{d}s q(\boldsymbol{r},s)\bar{q}(\boldsymbol{r},1-s) \tag{19}$$

$$\phi_B(\boldsymbol{r}) = \frac{Vc_P}{Q_P}\int_f^1 \mathrm{d}s q(\boldsymbol{r},s)\bar{q}(\boldsymbol{r},1-s) \tag{20}$$

$$\phi_S(\boldsymbol{r}) = \frac{Vc_S\sinh(p|\nabla\varphi(\boldsymbol{r})|)}{Q_S p|\nabla\varphi(\boldsymbol{r})|}\exp[-\omega_S(\boldsymbol{r})] \tag{21}$$

$$\sum_j \phi_j(\boldsymbol{r}) - 1 = 0 \tag{22}$$

where the propagator $q(\boldsymbol{r}, s)$, representing the probability of finding the s^{th} segment that starts from the A block end at position $\boldsymbol{r}$, satisfies the following modified diffusion equations ($R_g = b\sqrt{\frac{N}{6}} = 1$)

$$\frac{\partial q(\boldsymbol{r},s)}{\partial s} = \begin{cases} \nabla^2 q(\boldsymbol{r},s) - N[\omega_A(\boldsymbol{r}) + \alpha_A z_A e\varphi(\boldsymbol{r})]q(\boldsymbol{r},s) & \text{if } s\le f \\ \nabla^2 q(\boldsymbol{r},s) - N[\omega_B(\boldsymbol{r}) + \alpha_B z_B e\varphi(\boldsymbol{r})]q(\boldsymbol{r},s) & \text{if } s\ge f \end{cases} \tag{23}$$

with the initial condition $q(\boldsymbol{r}, 0) = 1$. Similarly, the backward propagator $\bar{q}(\boldsymbol{r},s)$, starting from the B block end, satisfies

$$\frac{\partial \bar{q}(\boldsymbol{r},s)}{\partial s} = \begin{cases} \nabla^2 \bar{q}(\boldsymbol{r},s) - N[\omega_B(\boldsymbol{r}) + \alpha_B z_B e\varphi(\boldsymbol{r})]\bar{q}(\boldsymbol{r},s) & \text{if } s\le 1-f \\ \nabla^2 \bar{q}(\boldsymbol{r},s) - N[\omega_A(\boldsymbol{r}) + \alpha_A z_A e\varphi(\boldsymbol{r})]\bar{q}(\boldsymbol{r},s) & \text{if } s\ge 1-f \end{cases} \tag{24}$$

with the initial condition $\bar{q}(\boldsymbol{r}, 0) = 1$.

The electrostatic potential is determined by a Poisson–Boltzmann equation, which is obtained by extremizing the free energy with respect to the electrostatic potential, *i.e.*, $\delta F/\delta\varphi = 0$

$$-\nabla\cdot\left[\frac{N\varepsilon(\boldsymbol{r})}{4\pi\rho_0\beta}\nabla\varphi(\boldsymbol{r})\right] = N\phi_e(\boldsymbol{r}) + \nabla\cdot\left[\frac{Np\phi_S(\boldsymbol{r})}{|\nabla\varphi(\boldsymbol{r})|}\mathrm{L}(p|\nabla\varphi(\boldsymbol{r})|)\nabla\varphi(\boldsymbol{r})\right] \tag{25}$$

where $\mathrm{L}(x) = \coth x - 1/x$ is a Langevin function. $\phi_e(\boldsymbol{r})$ is a summation over the charge densities of polyions and small ions at position $\boldsymbol{r}$, which is given as

$$\phi_e(\boldsymbol{r}) = \sum_{k=A,B}\alpha_k z_k e\phi_k(\boldsymbol{r}) + \phi_{+,e}(\boldsymbol{r}) + \phi_{-,e}(\boldsymbol{r}) \tag{26}$$

$$\phi_{\pm,e}(\boldsymbol{r}) = z_\pm e\frac{Vc_\pm}{Q_\pm}\exp[-\nu_\pm\omega_\pm(\boldsymbol{r}) - z_\pm e\varphi(\boldsymbol{r})] = \frac{z_\pm e}{\nu_\pm}\phi_\pm(\boldsymbol{r}) \tag{27}$$

By defining $\frac{N\varepsilon_{\text{eff}}(\boldsymbol{r})}{4\pi\rho_0\beta} = \frac{N\varepsilon(\boldsymbol{r})}{4\pi\rho_0\beta} + \frac{Np\phi_S(\boldsymbol{r})}{|\nabla\varphi(\boldsymbol{r})|}\mathrm{L}(p|\nabla\varphi(\boldsymbol{r})|)$, the Poisson–Boltzmann equation (eqn (25)) can then be written in a more general and condensed form

$$\nabla\cdot\left[\frac{N\varepsilon_{\text{eff}}(\boldsymbol{r})}{4\pi\rho_0\beta}\nabla\varphi(\boldsymbol{r})\right] = -N\phi_e(\boldsymbol{r}) \tag{28}$$

This equation is the typical Langevin Poisson–Boltzmann equation, as presented in Iglič's study.[31,32]

We applied the incompressibility on the whole system (without added salt), which gives

$$c_P + c_+\nu_+ + c_-\nu_- = c_P + c_P f\alpha_A\nu_+ + c_P(1-f)\alpha_B\nu_- = 1 - c_S \tag{29}$$

The free energy can be split into the contributions of internal energy U and entropy S, *i.e.*, $F = U - TS$, where $U = U_\chi + U_e$ and $S = S_P + S_S + S_+ + S_-$.[29,30,40,41] These terms possess the following expressions

$$\begin{aligned} \frac{NU_\chi}{\rho_0 Vk_B T} &= \frac{N}{2V}\int \mathrm{d}\boldsymbol{r}\sum_{\substack{j,j' \\ j\neq j'}}\chi_{jj'}\phi_j(\boldsymbol{r})\phi_{j'}(\boldsymbol{r}) \\ \frac{NU_e}{\rho_0 Vk_B T} &= \frac{1}{V}\int \mathrm{d}\boldsymbol{r}\frac{N\varepsilon(\boldsymbol{r})}{8\pi\rho_0\beta}|\nabla\varphi(\boldsymbol{r})|^2 \\ \frac{NS_P}{\rho_0 Vk_B} &= \frac{N}{V}\int \mathrm{d}\boldsymbol{r}\sum_{k=A,B}[\omega_k(\boldsymbol{r})\phi_k(\boldsymbol{r}) + \alpha_k z_k e\varphi(\boldsymbol{r})\phi_k(\boldsymbol{r})] + c_p\ln\left(\frac{Q_P}{V}\right) \\ \frac{NS_S}{\rho_0 Vk_B} &= \frac{N}{V}\int \mathrm{d}\boldsymbol{r}\left[\omega_S(\boldsymbol{r})\phi_S(\boldsymbol{r}) - \frac{\varepsilon_{\text{eff}}(\boldsymbol{r}) - \varepsilon(\boldsymbol{r})}{4\pi\rho_0\beta}|\nabla\varphi(\boldsymbol{r})|^2\right] + Nc_S\ln\left(\frac{Q_S}{V}\right) \\ \frac{NS_\pm}{\rho_0 Vk_B} &= \frac{N}{V}\int \mathrm{d}\boldsymbol{r}\left[\omega_\pm(\boldsymbol{r})\phi_\pm(\boldsymbol{r}) + \varphi(\boldsymbol{r})\phi_{\pm,e}(\boldsymbol{r})\right] + Nc_\pm\ln\left(\frac{Q_\pm}{V}\right) \end{aligned} \tag{30}$$

Numerical method

The self-consistent field equations were solved in real space, using a variant of the algorithms developed by Fredrickson and co-workers.[7,8,38,39] The diffusion equations (eqn (23) and (24)) were solved with the Baker–Hausdorff operator splitting formula proposed by Rasmussen *et al.*,[11,42] where the fast Fourier transforms were performed by the software package developed at MIT.[43] The Langevin Poisson–Boltzmann equation $\nabla\cdot\left[\frac{N\varepsilon_{\mathrm{eff}}(\boldsymbol{r})}{4\pi\rho_0\beta}\nabla\varphi(\boldsymbol{r})\right]=f(\boldsymbol{r})$ was solved by an *ad-hoc* direct spectral method, where the $f(\boldsymbol{r})$ was obtained by replacing the charge densities in the right hand side of eqn (28) by those of a previous iteration.[37] The detailed *ad-hoc* direct spectral method is given by

$$\varphi(\boldsymbol{r})=\mathrm{F}^{-1}\left[-\frac{i\boldsymbol{k}}{k^2}\cdot\mathrm{F}\left[\frac{4\pi\rho_0\beta}{N\varepsilon_{\mathrm{eff}}(\boldsymbol{r})}\mathrm{F}^{-1}\left[-\frac{i\boldsymbol{k}}{k^2}\cdot\mathrm{F}\left[f(\boldsymbol{r})\right]\right]\right]\right] \quad (31)$$

where F and F^{-1} represent forward and inverse Fourier transform operations. The above solution procedure involves four fast Fourier transforms and three multiplications for a total cost of $10M\log_2 M$ (M is the scale of the problem). This cost is much smaller than that of solving diffusion equations. Notably, there are a number of methods available for solving the Poisson–Boltzmann equations with the cost ranging from O(M) to O(M^3). For example, Yang *et al.* recently proposed a highly efficient multi-grid method, but there is no standard solver for this method.[23] The present method is also highly efficient as long as the $f(\boldsymbol{r})$ is smooth enough. More important, it can be easily solved by employing the FFTW packages. The densities $\phi_k(\boldsymbol{r})$ of k species, conjugated with the chemical potential fields $\omega_k(\boldsymbol{r})$, are evaluated with eqn (17)–(22). The chemical potential fields $\omega_k(\boldsymbol{r})$ and the electrostatic field $\varphi(\boldsymbol{r})$ were updated using a two-step Anderson mixing scheme, *i.e.*, to obtain a next guess for the iteration, we took two previous solutions into account in every iteration step.[44]

Since the present work is focused on lamellar structures, the unit-cell SCFT calculations were carried out in one dimension with periodic boundary conditions. In the calculations, the contour step sizes were set as $\Delta s=0.01$ and spatial resolutions were taken as $\Delta z<0.05R_{\mathrm{g}}$. The simulation continues until the relative accuracy in the fields (measured by $\sqrt{\sum_i\int\mathrm{d}\boldsymbol{r}(\omega_i^{\mathrm{new}}(\boldsymbol{r})-\omega_i^{\mathrm{old}}(\boldsymbol{r}))^2}\Big/\sum_i\int\mathrm{d}\boldsymbol{r}$) was smaller than 10^{-12} and a condition of incompressibility was achieved.[45,46] To obtain the stable structures, the free energy was minimized with respect to the sizes of the simulation box, as suggested by Bohbot-Raviv and Wang.[47]

Results and discussion

The developed SCFT was applied to determine the phase behavior of diblock polyampholytes ($\alpha_{\mathrm{A}}=\alpha_{\mathrm{B}}=\alpha$) and charged–neutral diblock copolymers ($\alpha_{\mathrm{A}}=0$ and $\alpha_{\mathrm{B}}=\alpha$) in polar solvents. The diblock polyelectrolytes were treated to have smeared charge distributions. For the simplicity of investigations, some parameters are fixed in the whole study: $\varepsilon_{\mathrm{A}}=\varepsilon_{\mathrm{B}}=\varepsilon_{\mathrm{S}}=\varepsilon_{+}=\varepsilon_{-}$, $\frac{N\varepsilon(\boldsymbol{r})}{4\pi\rho_0\beta}=1$, $f_{\mathrm{A}}=f_{\mathrm{B}}=0.5$, $N_{\mathrm{A}}=N_{\mathrm{B}}=N/2=200$, $\chi_{\mathrm{AB}}=0.3$, and $z_{\mathrm{A}}=z_{-}=-z_{\mathrm{B}}=-z_{+}=-1$. In addition, to avoid the complication resulting from possible macrophase separation, the polar solvents are assumed to be compatible with the polyelectrolytes, and we set $c_{\mathrm{P}}=0.8$ and $\chi_{\mathrm{AS}}=\chi_{\mathrm{BS}}=0$. Thus, the solution studied is in the concentrated regions.

The volume of ions is ignored in the calculations, *i.e.*, $\nu_{\pm}=0$ was chosen. Such a choice is due to the following two reasons. One is that the ions are much smaller than the polymer segments and solvents. The other is that we try to make the results comparable to those of ref. 20. We have tested the influence of $\nu_{\pm}$ on the phase behavior of diblock polyampholyte solutions. It was found that the $\nu_{\pm}$ has a less marked effect on the charge density distributions and order parameter profiles when the $\nu_{\pm}$ is smaller (see Fig. S1†). Only when the $\nu_{\pm}$ becomes much larger, does an obvious difference appear. For the charge density distributions, the main difference was found in the domain they dislike. Therefore, we think that the treatment of $\nu_{\pm}$ as 0 can approximate the cases of small ions well.

Solvation effect in diblock polyampholyte solutions

We first studied the microphase separation of diblock polyampholytes in the dipolar solvents, *i.e.*, the case of $\alpha_{\mathrm{A}}=\alpha_{\mathrm{B}}=\alpha$. Because of the symmetrical characteristic of such polyelectrolytes, the diblock polyampholyte solutions are able to form lamellar structures. Fig. 2 shows the effects of the magnitude of dipole moment p on the order parameter profiles $\phi_{\mathrm{A}}(z)-\phi_{\mathrm{B}}(z)$ of the systems with $\alpha=0.1$. With increasing the p value, the segregation between A and B blocks becomes strong, and this effect becomes less pronounced when the p is larger. For $p=0$, the LPB equation becomes the conventional PB equation as in ref. 20, and there is no dipolar effect imposed on the polyelectrolyte solutions. Therefore, the result for $p=0$ is completely consistent with that in ref. 20 (for the sake of comparison, the parameters chosen in this work are the same as those in ref. 20).

Because the diblock polyampholyte solutions are more segregated at higher p value, we might expect that the interaction strength $\chi_{\mathrm{ODT}}N$ at which order–disorder transition occurs would decrease with increasing the p value. We did find such

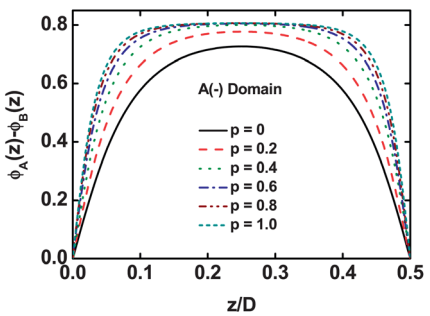

Fig. 2 Order parameter profiles $\phi_{\mathrm{A}}(z)-\phi_{\mathrm{B}}(z)$ of the lamellar structure of symmetric diblock polyampholytes in polar solvents. The degree α of ionization is fixed to be 0.1.

kinds of decrease, as presented in Fig. S2.† The results also show that the decrease of $\chi_{ODT}N$ upon increasing the p becomes more pronounced for the diblock polyampholyte solutions with larger α. When the p value is larger, the $\chi_{ODT}N$ approaches that of the neutral diblock copolymer solutions, implying that the charged objects are almost screened. The results indicate that the diblock polyampholyte solutions with higher magnitude of dipole moments can be microphase-separated at higher temperature, *i.e.*, lower χN.

Fig. 3 shows the effect of p on the charge density profiles of the systems with $\alpha = 0.1$. As shown in Fig. 3a, the total charge distributions exhibit an electric double layer near the A–B interface, where $z = 0$ or $z = 0.5$ corresponds to the A–B interface. The decay length is so long that the two double layers interfere with each other. These two double layers become less obvious as the p value increases. In addition, the total charge becomes more negative when the p is larger. In contrast to the total charge density distributions (centrosymmetry), the charge density distributions of counterions are asymmetric in the A and B domains, as shown in Fig. 3b. Since the positive counterions prefer to accumulate in the domain rich in negative A blocks, they show a higher charge density in A domains ($z < 0.5$). The charge density profiles of counterions exhibit a narrow peak in their preferred domain and a broad groove in the opposite domain. With increasing the p value, the charge density of counterions in their preferred domains decreases, while that in the opposite domain increases. This implies that the selectivity of free counterions to polymeric domains becomes less pronounced at higher p values.

In Fig. 4 we present the effective dielectric constant $\frac{N\varepsilon_{\text{eff}}(\boldsymbol{r})}{4\pi\rho_0\beta}$ as a function of the position z/D along the lamellar normal. The

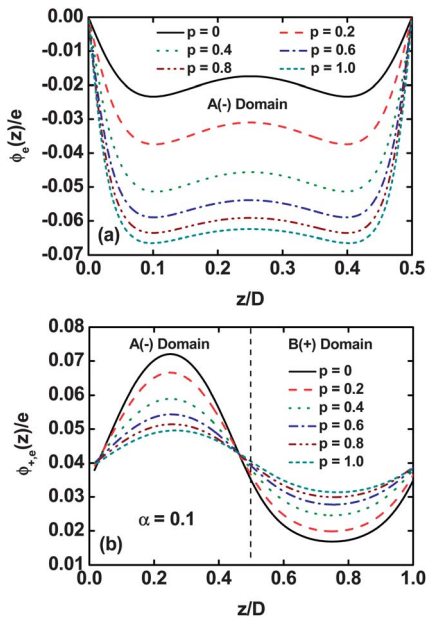

Fig. 3 (a) Total charge density profiles $\phi_e(z)/e$ and (b) charge density profiles $\phi_{+,e}(z)/e$ of positive counterions as a function of the direction z/D along the lamellar normal for the salt-free solutions of the diblock polyampholytes with $\alpha = 0.1$.

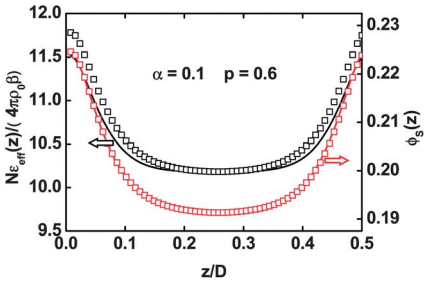

Fig. 4 Effective dielectric constant $N\varepsilon_{\text{eff}}(z)/(4\pi\rho_0\beta)$ and solvent density distribution $\phi_S(z)$ as a function of the direction z/D along the lamellar normal. The ionization degree α is 0.1, and the magnitude of the dipole moment p is 0.6. The solid lines are the results calculated by our method, and the square symbols are the results obtained from the calculation of SCFT equations with the Poisson–Boltzmann equation (without dipoles).

typical result manifested is for the system with $\alpha = 0.1$ and $p = 0.6$. Compared with the fixed medium dielectric constant $\frac{N\varepsilon(\boldsymbol{r})}{4\pi\rho_0\beta} = 1$ for the PB theory ($p = 0$), the effective dielectric constant in LPB calculations becomes inhomogeneous and shows a strong deviation, as shown in Fig. 4. This deviation occurs not only at the A–B interface, but also in the domains. We found that the $\frac{N\varepsilon_{\text{eff}}(\boldsymbol{r})}{4\pi\rho_0\beta}$ in the middle domain rises to above one order of $\frac{N\varepsilon(\boldsymbol{r})}{4\pi\rho_0\beta} = 1$ ($p = 0$), and becomes even larger near the A–B interface. For the larger p values, the $\frac{N\varepsilon_{\text{eff}}(\boldsymbol{r})}{4\pi\rho_0\beta}$ can rise to much higher orders, for example, the $\frac{N\varepsilon_{\text{eff}}(\boldsymbol{r})}{4\pi\rho_0\beta}$ at $p = 2$ is roughly two orders of $\frac{N\varepsilon(\boldsymbol{r})}{4\pi\rho_0\beta}$. Notably, the profile of the effective dielectric constant resembles that of the solvent density, as also shown in Fig. 4. This can be understood by reconsidering the formalism of the effective dielectric constant (eqn (28)). For weak fields ($p|\nabla\varphi| < 1$), one can expand the Langevin function in the equations into a first-order Taylor series, and thus obtain $\frac{N\varepsilon_{\text{eff}}(\boldsymbol{r})}{4\pi\rho_0\beta} \approx \frac{N\varepsilon(\boldsymbol{r})}{4\pi\rho_0\beta} + \frac{\phi_S(\boldsymbol{r})Np^2}{3}$. Seen from the Taylor series, it is clear that the effective dielectric constant is proportional to the solvent density $\phi_S(\boldsymbol{r})$. This is the main reason that both the effective dielectric constant and the solvent density have similar distribution profiles.

Since the effective dielectric constant follows the solvent distribution, it stands to reason that the same behavior may be obtained by solving the Poisson–Boltzmann equations with a position-dependent dielectric constant (without explicit solvent dipoles). This approximation is commonly used,[20,48–50] and we have tested the validity of this method. In terms of

$$\frac{N\varepsilon_{\text{eff}}(\boldsymbol{r})}{4\pi\rho_0\beta} \approx \frac{N\varepsilon(\boldsymbol{r})}{4\pi\rho_0\beta} + \frac{\phi_S(\boldsymbol{r})Np^2}{3} = \sum_{k=A,B}\phi_k(\boldsymbol{r})\frac{N\varepsilon_k}{4\pi\rho_0\beta} + \phi_S(\boldsymbol{r})\left(\frac{N\varepsilon_S}{4\pi\rho_0\beta} + \frac{Np^2}{3}\right),$$

we took the dielectric constant of the solvents as $\frac{N\varepsilon_{S,\text{eff}}}{4\pi\rho_0\beta} = \frac{N\varepsilon_S}{4\pi\rho_0\beta} + \frac{Np^2}{3}$. This dielectric constant $\frac{N\varepsilon_{S,\text{eff}}}{4\pi\rho_0\beta}$ is much

larger than those of the polymers. Through calculating the SCFT equations with the conventional PB equation, we obtained the distributions of the solvents and the dielectric constant. The calculation results are incorporated into Fig. 4. As shown in the figure, the solvent densities obtained by these two methods are well fitted, although the effective dielectric constants are slightly different. This implies that the approaches by considering only a varying dielectric constant are capable of capturing the (structural) behavior of polyelectrolytes in concentrated solutions. Strictly speaking, this approximation approach can be more effective when $p|\nabla\varphi| \rightarrow 0$ (see Section 3 of the ESI†). However, it should be emphasized that the dielectric constants in this approach are usually qualitative, and there is no unambiguous method to evaluate the dielectric constants of the dipolar medium. Rather, our study has provided a way to evaluate the effective dielectric constant based on the knowledge of the dielectric constant and the magnitude of the dipole moment. The obtained effective dielectric constant, including an implicit ion–dipole interaction, can be used as an input for the approaches involving only a varying dielectric constant and no ion–dipole interactions.

Fig. 5 shows the lamellar spacing D/R_g as a function of p for the polyelectrolytes with various degrees α of ionization. It can be seen from Fig. 5 that, for all cases, the lamellar spacing first slightly decreases and then rapidly increases to a plateau, as the p value increases. With increasing the α value, the lamellar spacing shows a dramatic decrease at lower p value and a slight decrease at higher p value. As a result, the changes of lamellar spacing, responding to the change of the p value, become more dramatic as the α value is higher. It is worth noting that, at higher p value, the lamellar spacing reaches a plateau value of $D = 5.60R_g$, which is the lamellar spacing of the neutral diblock copolymers in solutions. This suggests that the charges are almost screened by the polar solvents when the p value is higher.

The results shown in Fig. 2–5 have provided significant insight into the dependence of the phase behavior of diblock polyampholytes on the magnitude of dipole moment p. Regarding the nonpolar solvents ($p = 0$), the A and B blocks carrying opposite charges attract each other, which leads to a narrower spacing (Fig. 5) and broader interfacial width (Fig. 2), at the expense of the interaction energy between the incompatible blocks. Moreover, the free counterions are mainly distributed in the domain rich in the blocks with opposite charges (Fig. 3). In this way, the charged polymeric chain gets shielded by the mobile counterions. When the polar solvents with various magnitudes of dipole moments are introduced, they orient themselves to the charged objects including free counterions and a charged polymeric chain, giving rise to a screening of the charged objects. The screen effect is reflected by an increase of the effective dielectric constant, which is shown in Fig. 4. As a consequence, the electrostatic attraction between the A and B blocks decreases, and the unfavorable interaction enthalpy drives them to be more separated (Fig. 2) and stretched (large spacing, Fig. 5). In addition, the translational entropy drives the free counterions away from their preferred domains, resulting in a more homogeneous distribution (Fig. 3b). When the magnitude of dipole moments increases, the charged objects become more screened, and therefore the above phenomena are more evident. At higher magnitude of dipole moments, the charged objects are completely shielded, and the diblock polyampholytes thus perform much like the neutral polymers, for example, their lamellar spacings are nearly equal. However, there still remains the question as to why the lamellar spacing decreases at the onset of increasing the magnitude of dipole moments (see Fig. 5).

To address this question, we examined the enthalpic U and entropic S contributions to the free energy of the systems. Three cases for the diblock polyampholyte solutions with $\alpha = 0.06$ were considered, *i.e.*, $p = 0$, $p = 0.2$, and $p = 0.4$. The equilibrium spacings of the lamellae at $p = 0$, $p = 0.2$, and $p = 0.4$ are $2.82R_g$, $2.64R_g$, and $2.82R_g$, respectively. Table 1 shows the various enthalpic and entropic contributions to free energy for these three cases. The terms presented in the table are the differences between the contributions at $D = 2.82R_g$ and $D = 2.64R_g$, for example, $\Delta U_\chi = U_\chi(D = 2.82R_g) - U_\chi(D = 2.64R_g)$. Thus, a negative value implies that the contribution to the free energy decreases with increasing the lamellar spacing.

From the table, we can see that for all three cases, the internal energy U_χ and entropic loss $-S_P$ of the polyelectrolytes dramatically decrease with the increase in lamellar spacing. This implies that the formation of lamellae with larger spacing is favored by the internal energy U_χ and conformational entropy of the polyelectrolytes. However, the translational entropy S_I (*i.e.*, $S_+ + S_-$) of free counterions would decrease as the lamellar spacing increases. This is due to the fact that the free counterions are adsorbed to the polymeric domains carrying opposite charges, which restricts their translations. Such a restricted effect becomes less marked as the lamellar spacing decreases (reduced separation) or as the p value increases (reduced adsorption). Compared with the $p = 0$ case, when forming lamellae with larger spacing at $p = 0.2$, the loss of the translational entropy $-S_I$ of the counterions becomes more pronounced, and the electrostatic energy U_e becomes less favorable. This is the reason that the lamellar spacing decreases at the onset of increasing the p value. At higher p value ($p = 0.4$),

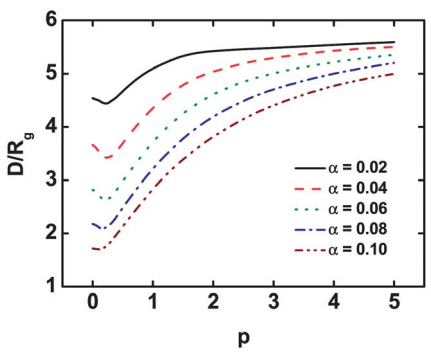

Fig. 5 Lamellar spacing D/R_g as a function of the magnitude of dipole moments p for the salt-free solutions of diblock polyampholytes with various degrees α of the ionizations.

Table 1 The differences of free energy $\Delta F/nk_BT$, internal energy $\Delta U_\chi/nk_BT$, electrostatic energy $\Delta U_e/nk_BT$, entropic loss $-\Delta S_P/nk_B$ of the polyelectrolytes, entropic loss $-\Delta S_S/nk_B$ of the solvents, and entropic loss $-\Delta S_I/nk_B$ ($S_I = S_+ + S_-$) of the counterions for diblock polyampholytes with $\alpha = 0.06$ ($n = \rho_0 V/N$). The differences are given as $\Delta f_n = f_n(D = 2.82R_g) - f_n(D = 2.64R_g)$, where $f_n = F, U_\chi, U_e, -S_P, -S_S, -S_I$. $D = 2.82R_g$ is the equilibrium lamellar spacing for the $p = 0$ and $p = 0.4$ cases, while $D = 2.64R_g$ is the equilibrium lamellar spacing for the $p = 0.2$ case

	$\Delta F/nk_BT$	$\Delta U_\chi/nk_BT$	$-\Delta S_P/nk_B$	$\Delta U_e/nk_BT$	$-\Delta S_S/nk_B$	$-\Delta S_I/nk_B$
$p = 0$	−0.00968	−0.17526	−0.09941	−0.04564	−0.00234	0.31298
$p = 0.2$	0.01348	−0.20596	−0.13653	−0.00413	−0.01049	0.3706
$p = 0.4$	−0.01642	−0.15994	−0.11717	0.01417	0.05593	0.1906

the change of the translational entropy of the counterions becomes less marked (reduced adsorption due to the screening) and thereby, the internal energy U_χ and the conformational entropy S_P of the polyelectrolytes dominate the formation of the structures. As a result, the lamellar spacing increases.

Solvation effect in charged–neutral diblock copolymer solutions

While the above calculations are focused on the $\alpha_A = \alpha_B$ cases, we extended the calculations for $\alpha_A = 0$ cases. Therefore, the system studied becomes a salt-free solution of charged–neutral diblock copolymers, which is another system that researchers are interested in.[23] Fig. 6 shows the dependence of the order parameter profiles on p for the charged–neutral diblock copolymer solutions with $\alpha_B = 0.08$. As can be seen from Fig. 6, the p values have a less pronounced influence on the order parameter profiles. This is due to the fact that the charged–neutral diblock copolymers always remain well-segregated when the magnitude of the dipole moment changes. However, we can still identify from the enlarged profiles at the interface that the segregation between the A and B blocks becomes strong with increasing the magnitude of dipole moments, although such a change is less marked.

In contrast with the order parameters, the charge density distributions of the charged–neutral diblock copolymers are greatly dependent on the p value. Fig. 7a shows the dependence of the total charge density distributions on the p values. Because of the asymmetric ionizable degrees of the A and B blocks, the total charge density profiles in the A ($z < 0.5$) and B ($z > 0.5$) domains are also asymmetric. The total charge densities in the ionizable B domains are positive, while those in the non-ionizable A domain are negative. The interfered electric double layers were also observed in both domains. As the p value increases, the total charge densities become more positive in the ionizable B domain and more negative in the neutral A domains. The change of total charge density distribution arises mainly from the redistribution of free counterions (negative) as a function of the p values. Fig. 7b presents the density profiles $\phi_{-,e}(z)/(z_-e)$ of the negative counterions. As can be seen, the negative counterions are mainly distributed in the domain rich in the ionizable B blocks due to the electrostatic adsorption. The density shows a decrease ranging from the center of the B domain ($z/D = 0.75$) to the middle of A domains ($z/D = 0.25$). With increasing the p values, the density distributions become flat, namely, the density of the negative counterions decreases in the B domain but increases in A domains. In this sense, the free counterions and the ionizable B blocks are screened by the polar solvents when the magnitude of the dipole moment increases. As a result, the translational entropy drives the free negative counterions to be distributed more uniformly (Fig. 7b), leading to a lower total charge density in the neutral A domains and a higher total charge density in the ionizable B domains (Fig. 7a).

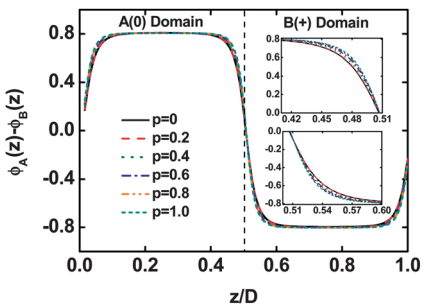

Fig. 6 Order parameter profiles $\phi_A(z) - \phi_B(z)$ of the lamellar structure of charged–neutral diblock copolymers ($\alpha_A = 0$ and $\alpha_B = 0.08$) in polar solvents. The insets show the enlarged profiles of order parameters.

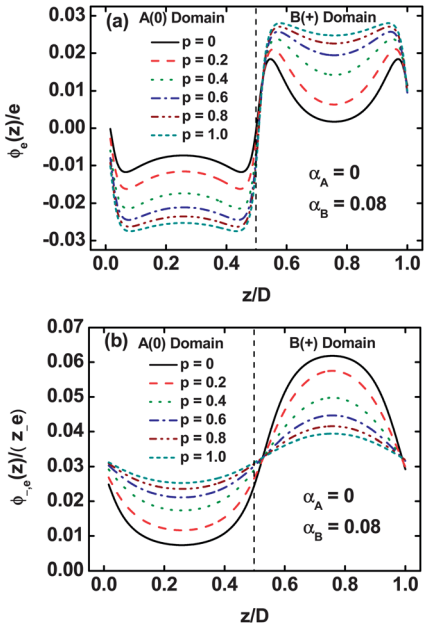

Fig. 7 (a) Total charge density profiles $\phi_e(z)/e$ and (b) density profiles $\phi_{-,e}(z)/(z_-e)$ of negative counterions as a function of the direction z/D along the lamellar normal for the salt-free solutions of charged–neutral diblock copolymers with $\alpha_A = 0$ and $\alpha_B = 0.08$.

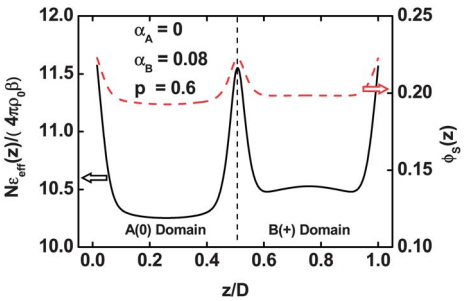

Fig. 8 Effective dielectric constant $N\varepsilon_{eff}(z)/(4\pi\rho_0\beta)$ and solvent density distribution $\phi_S(z)$ as a function of the direction z/D along the lamellar normal. The ionization degrees are $\alpha_A = 0$ and $\alpha_B = 0.08$, and the magnitude of the dipole moment is $p = 0.6$.

The screen effects are reflected as the increase in the effective dielectric constant. Shown in Fig. 8 is the dielectric constant as a function of the direction z/D normal to the lamella. The $\frac{N\varepsilon_{eff}(\boldsymbol{r})}{4\pi\rho_0\beta}$ at $p = 0.6$ are found to be about 10 times higher than the $\frac{N\varepsilon(\boldsymbol{r})}{4\pi\rho_0\beta}$ value. In addition, the $\frac{N\varepsilon_{eff}(\boldsymbol{r})}{4\pi\rho_0\beta}$ is no longer symmetric in the A and B domains. The effective dielectric constant in the ionizable B domain is slightly higher than that in the neutral A domain, and the maximum effective dielectric constant appears at the interface. The profile also resembles that of the solvent density distribution (red line). The appearance of relatively higher solvent density in the ionizable B domain may be due to the electrostatic adsorption between the charged B blocks and dipolar solvents.

The lamellar spacing of the charged–neutral diblock copolymer solutions at various magnitudes of the dipole moments was also examined. The result is presented in Fig. 9. As shown in Fig. 9, the variation of the lamellar spacing as a function of the magnitude of dipole moments is similar to that of diblock polyampholyte solutions (see Fig. 5). The main difference between these two cases is the absolute magnitude of the spacing at lower p values. We can see that the spacing of charged–neutral diblock copolymer solutions at lower p is significantly larger than that of diblock polyampholyte solutions, because the electrostatic adsorption between the A and B blocks is absent in the solutions of charged–neutral diblock copolymers. At higher p value, this difference becomes less marked, since the charged objects are almost shielded by the polar solvents. For example, when $p = 5.0$, the lamellar spacing of both the charged–neutral diblock copolymer solutions with $\alpha_A = 0.02$ and the diblock polyampholyte solutions with $\alpha_A = \alpha_B = 0.02$ have the same value of about $5.6R_g$.

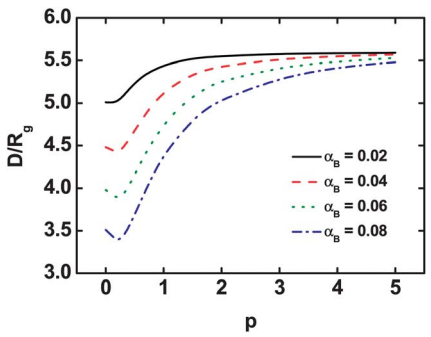

Fig. 9 Lamellar spacing D/R_g as a function of the magnitude of dipole moment p for the salt-free solutions of charged–neutral diblock copolymers with $\alpha_A = 0$.

While making a comparison between the two polyelectrolyte systems, we learned that the effect of the magnitude of the dipole moment on the phase behaviors has some similarity. For both cases, the segregation between dissimilar blocks becomes strong, and the lamellar spacing shows similar non-monotonic variations as the magnitude of the dipole moment increases. However, there also exist some differences. Compared with the diblock polyampholyte systems, the variations of spacing and segregation as a function of the magnitude of the dipole moment become less marked in the charged–neutral diblock copolymer solutions. In addition, the effective dielectric constant in different domains is asymmetric in the charged–neutral diblock copolymer solutions, while it is symmetric in the diblock polyampholyte solutions. These differences mainly result from the absence of charges in one block of the charged–neutral diblock copolymers.

The present calculations demonstrate that the polar solvents such as the water play an important role in determining the structures and properties of polyelectrolyte solutions. For weak polyelectrolytes ($p|\nabla\varphi| < 1$), this behavior can also be captured by setting the dielectric constant of solvents to be $\frac{N\varepsilon_{S,eff}}{4\pi\rho_0\beta} = \frac{N\varepsilon_S}{4\pi\rho_0\beta} + \frac{Np^2}{3}$, using the SCFT with the conventional PB equation. This quantitative relationship is obtained from the LPB equation. The LPB equation in the present method is similar to those developed by Orland *et al.* and Iglič *et al.*,[31–36] but it shows some differences. The solvent density is a variable in the present LPB equation, while remaining constant in their formalisms. In their calculations, they found that the effective dielectric constant decreases around the charged objects due to the increased strength of the electric field, according to the second-order expansion of the effective dielectric constant $\frac{N\varepsilon_{eff}(\boldsymbol{r})}{4\pi\rho_0\beta} = \frac{N\varepsilon(\boldsymbol{r})}{4\pi\rho_0\beta} + \frac{\phi_S Np^2}{3} - \frac{\phi_S Np^2(p|\nabla\varphi|)^2}{45}$. However, since the solvent density ϕ_S is variable in the present formalism, the second term in the right-hand side of the above equation plays a predominant role, and thereby the effective dielectric constant resembles the profile of the solvent density.

After finishing this work, we noted a work carried out by Kumar *et al.*[51] This recent published work focuses on charge regulation and local dielectric function in planar polyelectrolyte brushes, by considering explicit ion–dipole interactions. From this work, we learned that the present method can be further generalized to the systems containing other ion–dipole interactions, such as the polyelectrolyte systems involving counterion adsorption. Since the magnitude of dipole moments was fixed in their work, the effect of the magnitude of dipole moments on the behavior of polyelectrolytes is still unclear. In this study, we provided a comprehensive study of such an effect, and a non-monotonic variation of the lamellar spacing was found.

Conclusions

We developed a SCFT coupled with the LPB equations for studying the polyelectrolytes in polar solvents. The LPB equation was derived to describe the electrostatic interactions such as ion–dipole interactions in polyelectrolyte solutions, by modeling the polar solvents as Langevin dipoles. From the LPB equation, we learned that the effective dielectric constant is related to the solvent density, the magnitude of dipole moments, and the strength of the electric field. The LPB equation is numerically solved using an *ad-hoc* direct spectral method, which is proved to be highly effective in the framework of real-space SCFT. The method was tested for two types of polyelectrolytes – diblock polyampholytes and charged–neutral diblock copolymers. It was found that the effective dielectric constant increases as the magnitude of the dipole moment increases. The profile of the effective dielectric constant is similar to that of the solvent distributions, indicating that the solvent density plays a dominant role in these systems. Since the higher effective dielectric constant can lead to the screening of more charged objects by the polar solvents, the segregation between dissimilar blocks becomes stronger at higher magnitude of the dipole moment. In addition, the lamellar spacing undergoes a non-monotonic variation – first it decreases and then it increases to infinitely approach the spacing of the neutral diblock copolymers in solvents, as the magnitude of the dipole moment increases.

Acknowledgements

This work was supported by the National Natural Science Foundation of China (50925308, 21234002), the Key Grant Project of the Ministry of Education (313020) and the National Basic Research Program of China (no. 2012CB933600). Support from the project of Shanghai municipality (10GG15) is also appreciated.

References and notes

1 M. Hara, in *Polyelectrolytes: Science and Technology*, Marcel Dekker Inc., New York, 1993.
2 T. Radeva, in *Physical Chemistry of Polyelectrolytes*, Marcel Dekker Inc., New York, 2001.
3 M. Schmidt, in *Polyelectrolytes with Defined Molecular Architectures*, Springer-Verlag, Berlin Heidelberg, 2004.
4 D. Andelman, in *Handbook of Biological Physics: Structure and Dynamics of Membranes*, Elsevier Science, B. V. Amsterdam, 1995.
5 S. F. Edwards, *J. Phys. A: Math. Gen.*, 1975, **8**, 1670.
6 M. Doi and S. F. Edwards, in *The Theory of Polymer Dynamics*, Clarendon Press, Oxford, 1986.
7 G. H. Fredrickson, in *The Equilibrium Theory of Inhomogeneous Polymers*, Oxford University Press, Oxford, U.K., 2006.
8 F. Drolet and G. H. Fredrickson, *Macromolecules*, 2001, **34**, 5317–5324.
9 M. W. Matsen and R. B. Thompsom, *J. Chem. Phys.*, 1999, **111**, 7139–7146.
10 F. Schmid, *J. Phys.: Condens. Matter*, 1998, **10**, 8105–8138.
11 K. Ø. Rasmussen and G. Kalosakas, *J. Polym. Sci., Part B: Polym. Phys.*, 2002, **40**, 1777–1783.
12 J. Y. Lee, R. B. Thompson, D. Jasnow and A. C. Balazs, *Macromolecules*, 2002, **35**, 4855–4858.
13 R. B. Thompson, V. V. Ginzburg, M. W. Matsen and A. C. Balazs, *Macromolecules*, 2002, **35**, 1060–1071.
14 L. Wang, J. Lin and L. Zhang, *Macromolecules*, 2010, **43**, 1602–1609.
15 L. Zhang and J. Lin, *Macromolecules*, 2009, **42**, 1410–1414.
16 J. Hubbard, *Phys. Rev. Lett.*, 1959, **3**, 77–80.
17 I. Borukhov, D. Andelman and H. Orland, *Eur. Phys. J. B*, 1998, **5**, 869–880.
18 I. Borukhov, D. Andelman and H. Orland, *Europhys. Lett.*, 1995, **32**, 499–504.
19 A.-C. Shi and J. Noolandi, *Macromol. Theory Simul.*, 1999, **8**, 214–229.
20 Q. Wang, T. Taniguchi and G. H. Fredrickson, *J. Phys. Chem. B*, 2004, **108**, 6733–6744; 2005, **109**, 9855–9856.
21 R. Kumar and M. Muthukumar, *J. Chem. Phys.*, 2007, **126**, 214902.
22 S. Yang, A. Vishnyakov and A. V. Neimark, *J. Chem. Phys.*, 2011, **134**, 054104.
23 Y. Liu, H. Zhang, C. Tong and Y. Yang, *Macromolecules*, 2011, **44**, 8261–8269.
24 Q. Wang, *J. Phys. Chem. B*, 2006, **110**, 5825–5828.
25 Q. Wang, *Macromolecules*, 2005, **38**, 8911–8922.
26 C. Tong, Y. Zhu, H. Zhang, F. Qiu, P. Tang and Y. Yang, *J. Phys. Chem. B*, 2011, **115**, 11307–11317.
27 K. N. Witte and Y. Y. Won, *Macromolecules*, 2006, **39**, 7757–7768.
28 L.-J. Qu, X. Jin and Q. Liao, *Macromol. Theory Simul.*, 2009, **18**, 162–170.
29 R. Kumar and M. Muthukumar, *J. Chem. Phys.*, 2008, **128**, 184902.
30 R. Kumar, A. Kundagrami and M. Muthukumar, *Macromolecules*, 2009, **42**, 1370–1379.
31 E. Gongadze, U. van Rienen, V. Kralj-Iglič and A. Iglič, *Gen. Physiol. Biophys.*, 2011, **30**, 130–137.
32 A. Iglič, E. Gongadze and K. Bohinc, *Bioelectrochemistry*, 2010, **79**, 223–227.
33 A. Abrashkin, D. Andelman and H. Orland, *Phys. Rev. Lett.*, 2007, **99**, 077801.
34 D. H. Mengistu, K. Bohinc and S. May, *Europhys. Lett.*, 2009, **88**, 14003.
35 P. Koehl, H. Orland and M. Delarue, *Phys. Rev. Lett.*, 2009, **102**, 087801.
36 P. Koehl and M. Delarue, *J. Chem. Phys.*, 2010, **132**, 064101.
37 C. Canuto, A. Quarteroni, M. Y. Hussaini and T. A. Zang, *Spectral Methods: Fundamentals in Single Domains*, Springer-Verlag, Berlin Heidelberg, 2006.
38 F. Drolet and G. H. Fredrickson, *Phys. Rev. Lett.*, 1999, **83**, 4317–4320.
39 V. Ganesan and G. H. Fredrickson, *Europhys. Lett.*, 2001, **55**, 814–820.

40 P. D. Gujrati and A. I. Leonov, *Modeling and Simulation in Polymers*, Wiley-VCH Verlag GmbH & Co. KGaA, Weinheim, 2010, p. 325.
41 F. Schwabl, *Statistical Mechanics*, Springer-Verlag, Berlin Heidelberg, 2006.
42 G. Tzeremes, K. Ø. Rasmussen, T. Lookman and A. Saxena, *Phys. Rev. E: Stat. Phys., Plasmas, Fluids, Relat.*, 2002, **65**, 041806.
43 FFTW, http//www/fftw.org/.
44 V. Eyert, *J. Comput. Phys.*, 1996, **124**, 271–285.
45 J. U. Kim and M. W. Matsen, *Soft Matter*, 2009, **5**, 2889–2895.
46 L. Wang and J. Lin, *Soft Matter*, 2011, **7**, 3383–3391.
47 Y. Bohbot-Raviv and Z.-G. Wang, *Phys. Rev. Lett.*, 2000, **85**, 3428–3431.
48 C. L. Ting, J. Wu and Z.-G. Wang, *Proc. Natl. Acad. Sci. U. S. A.*, 2011, **108**, 16986–16991.
49 C. L. Ting and Z.-G. Wang, *Biophys. J.*, 2011, **100**, 1288–1297.
50 O. A. Croze and M. E. Cates, *Langmuir*, 2005, **21**, 5627–5638.
51 R. Kumar, B. G. Sumpter and S. Michael Kilbey II, *J. Chem. Phys.*, 2012, **136**, 234901.